Poly(Vinylidene Difluoride) Soft Dendritic Colloids as Li-Ion Battery Separators

Journal of The Electrochemical Society, 2021 **168** 020517

Poly(Vinylidene Difluoride) Soft Dendritic Colloids as Li-Ion Battery Separators

Salvatore Luiso,[1,*,z] Austin H. Williams,[1] Michael J. Petrecca,[1,*] Sangchul Roh,[2] Orlin D. Velev,[1] and Peter S. Fedkiw[1,,z]**

[1]*Department of Chemical and Biomolecular Engineering, North Carolina State University, Raleigh, North Carolina 27695, United States of America*
[2]*Smith School of Chemical and Biomolecular Engineering, Cornell University, Ithaca, New York, United States of America*

As an alternative to Li-ion battery (LIB) microporous membrane separators that are typically comprised of polyolefins, other materials and separator morphologies may yield increased cell performance. Here, we present a new class of LIB separators comprising poly(vinylidene difluoride) (PVDF)-based and highly branched, colloidal polymer particulates, called soft dendritic colloids, that are produced by shear-driven polymer precipitation within a turbulent nonsolvent flow followed by filtration. We show the morphology of the resulting PVDF particulates may be varied from fibrous dendritic colloids to thin and highly porous sheet-like particles. The use of PVDF leads to low thermal shrinkage (5% at 90 °C) and high tensile strength (<0.7% offset at 1000 psi), while the high porosity (up to 80%) and high particle surface area are responsible for high conductivity (1.2 mS cm^{-1}) and electrolyte uptake (325%), and good cell capacity (112 mAh g^{-1} in Li/$LiCoO_2$ cell) with <10% loss after 50 cycles. Because shear-driven precipitation with filtration is a facile and versatile process to make a new class of polymeric LIB separators, soft dendritic colloids are promising candidates as separators for next-generation batteries.
 [DOI: 10.1149/1945-7111/abdfa7]

Manuscript submitted November 11, 2020; revised manuscript received January 17, 2021. Published February 5, 2021.

Supplementary material for this article is available online

LIBs are an essential energy storage system for a variety of applications because of their high energy-storage capabilities and long cycle life, comprising a $30 billion market as of 2017.[1–3] The LIB separator market was $2.6 billion with a compound annual growth rate of 14% at the end of 2017, and it's projected to reach $8 billion by 2030.[3] The structure and properties of the separator play a critical role in cell performance. The separator must be chemically and electrochemically stable and is usually not ionically conductive by itself; a liquid electrolyte imbibed within it effects ion transport. Indeed, the wettability of the separator by liquid electrolyte is important to affect high-ionic conductivity.[4] Good wettability permits rapid absorption of the electrolyte in the separator during cell assembly. A desirable battery separator is characterized by low ionic resistance, mechanical and thermal stability, and high affinity and wettability by electrolyte.[5] While separators may be classified according to their structure,[6] recent developments tend to classify them as single- or multi-layered, ceramic-based, or surface-modified separators.[7] Polyolefin monolayer microporous separators are the most widely used, but their hydrophobic surface with low surface energy exhibits poor affinity to polar organic electrolytes, and they need surfactants to obtain good electrolyte wettability.[8,9] Table SI (supplemental material) summarizes pertinent information about separators highlighted in the studies discussed below.

Relative to conventional microporous polyolefin separators, fibrous polymeric membranes, such as electrospun nonwovens, have the advantage of low mass and high porosity; in addition, the fibrous mat provides good structural cohesion due to intertwined fibers.[10–14] Although most polymers used to make fibrous battery separators have resulted in lower cell performance (lower ionic conductivity and, hence higher resistance) than conventional microporous separators, PVDF shows promising results because of its high polarity and good chemical stability and affinity for electrolytes commonly employed in Li-ion cells, owing to the presence of C–F groups.[15–22] PVDF is often used as a copolymer with hexafluoropropylene (HFP) to decrease the degree of crystallinity, and hence increase electrolyte uptake and ionic conductivity, but may decrease the mechanical and thermal properties of the separator; it is often necessary to create blends and composites of PVDF.[23–25] Nano-scale sized, electronically insulating metal oxides, such as SiO_2, Al_2O_3 and SnO_2,[26] LLZTO[27] or silicone[28] may be incorporated in the separator to increase membrane and cell performance, but often with non-scalable or expensive techniques, such as a sol-gel method,[29] in situ deposition, film casting,[15] physical vapor deposition,[30] or electrophoretic deposition.[31]

A different approach to improve PVDF-based membranes is to optimize their morphology, with scalable preparation processes and without the use of composites and blends. In previous work, we prepared PVDF membranes for the first time via meltblowing, a well-established mass-production process for creating mats/membranes, and we found that interactions between the PVDF fibers and electrolyte (1 M $LiPF_6$ in EC/DMC) increase uptake and conductivity.[32] Luo et al.[33] have prepared polyethylene/PVDF-HFP separators through a solvent liberation method. The variation in solvent evaporation rate between N-methyl pyrrolidone and acetone creates a hierarchical structure in the membrane with high porosity and ionic conductivity. The authors attribute a lower cell-capacity loss using these membranes to an inter-island structure formed in the membrane during the processing steps.[34] With a similar idea, Ye et al.[35] improved PVDF-HFP separators with an inter-particle chain structure. After casting the polymer from acetone and applying an electrolyte soaking and drying procedure, the authors report that the polymer chains rearrange toward a high density and highly porous structure. The interactions between solvents and non-solvents influence the formation of pores and phase transformation process,[33,36] leading to different morphologies, such as sponge-like or finger-like with an asymmetric distribution of pores.[7,22]

A new method of fabricating nanofibrous material in which a polymer solution is injected into a sheared nonsolvent flow has shown that polymer particulates may be produced in a continuous, scalable process using a laminar nonsolvent flow to elongate unidirectionally the polymer droplet into a fiber.[37,38] Additionally, the transition of the nonsolvent flow from laminar to turbulent regime alters the morphology of the resulting particulates and may produce highly branched soft dendritic colloids (SDCs), which are

*Electrochemical Society Student Member.
**Electrochemical Society Fellow.
[z]E-mail: sluiso@ncsu.edu; fedkiw@ncsu.edu

characterized by a corona of nanofibers surrounding the core of a particle.[39,40] The concentration of polymer in the injection solution dictates the morphology of the resulting particulates, with a low concentration resulting in fibrous morphologies, a high concentration resulting in thin, nano-sheet (NS) morphologies, and an intermediate concentration with combined fibrous-NS morphologies; the concentration at which the morphology transition happens is polymer dependent. In this work, we show that separators produced by vacuum filtration of solutions of shear-driven PVDF particulates, called here PVDF SDC separators, find application as efficient, versatile, and stable LIB separators. We investigate how cell performance may be effected by particle morphology in the SDC-based separator.

Experimental

Materials.—We use polyvinylidene fluoride (PVDF, Sigma Aldrich, Mw = 530,000 Da, PDI = 2.0), dimethyl sulfoxide (DMSO, Fisher Scientific) and ethanol (EtOH, Koptek) in this study. A Millipore vacuum filtration apparatus with a head diameter of 35 mm was used to filter particulate suspensions in EtOH.

Fabrication of PVDF SDC membranes.—PVDF pellets were dissolved in DMSO at various weight percentage of polymer by heating at 110 °C for 24 h while stirred. Following dissolution, the PVDF solution was cooled to room temperature and injected at a rate of $\sim$1 ml s^{-1} directly through a capillary into the shear zone of a colloidal mill (IKA Magic Lab) set to 20,000 rpm and filled with 500 ml of EtOH at room temperature. The resulting PVDF SDC suspensions were washed by centrifugation at 3.0 relative centrifugal force for 2 min, and discarding the supernatant, and the concentrated particles were resuspended in 40 ml EtOH using a Vortex mixer. This process was repeated a minimum of five times to remove DMSO. The suspension was adjusted to 0.1 wt.% PVDF in EtOH and a known volume of the solution was deposited on a Durapore® filtration membrane (0.45 micron pore size, 47 mm diameter) using a Millipore vacuum filtration apparatus. The suspension was vacuum filtered for 30 min to form the membrane. Samples were removed from the filtration funnel, sandwiched between two glass slides, and placed in an oven at 70 °C for 24 h to remove residual ethanol.

Microscopy and tensile strength.—The morphology of SDC particles and membranes formed from them were examined by field emission scanning electron microscopy (FEI-SEM, Verios 460L). We performed tensiometry on the membranes using a universal testing machine (Instron 4593) with 15 mm × 10 mm samples of varying thickness (15–50 μm) and a crosshead speed of 15 mm min^{-1}. A minimum of 4 replicas per membrane were measured.

Capillary flow porosimetry and porosity.—The inter-fiber spacing (pore) size was analyzed with an in-plane porometer (Porous Materials Inc.). Each sample was imbibed with a highly wetting liquid (Galwick®) with a known surface tension of 15.9 dynes cm^{-1}. No visible contact angle was detected, so we assumed a contact angle of 0° to calculate the pore diameter from the Young–Laplace equation: $D = 4\gamma_{L/G} \cos\theta/p$, where p is the extrusion pressure in MPa, D is the pore diameter in mm, $\gamma_{L/G}$ is the surface tension of Galwick in N mm^{-1}, and θ is the contact angle of Galwick with the sample. The porometer provides the population of pores with a specific diameter at each static pressure applied by the instrument during the measurement. Using the approach to calculate the number-average molecular weight (M_n), weight-average molecular weight (M_w), and polydispersity index (PDI = M_w/M_n) of a polymer, we calculated the equivalent number-average pore size (P_n), weight-average pore size (P_w), and heterogeneity index (HG = P_w/P_n).[39] Porosity was calculated as the complement of the ratio of geometrical density to fiber density: $P = 1 - \left(\frac{W}{t\rho_{fiber}}\right)$, where W is the basis weight (g cm^{-2}), t is the mat thickness (cm), and ρ_{fiber} = 1.78 g cm^{-3} is the density of PVDF. A minimum of 4 replicas per membrane were measured.

Thermal stability.—In a sequential process the SDC membranes were placed in an oven with air at 90 °C for 1 h, imaged, heated to 130 °C for 1 h, imaged, and lastly heated at 150 °C for 1 h, and imaged. The shrinkage of the membranes was determined using pixel analysis of photographs of the membranes using ImageJ software. We also used a thermogravimetric analyzer (SDT 650, TA Instruments) to determine the thermal decomposition temperature of PVDF SDC membranes.

Electrolyte uptake.—Because the electrolyte uptake by the PVDF membranes was fast (<1 s), we did not perform rate-of-wettability measurements. We determined electrolyte uptake with Eq. 1 by weighing the separators before and after soaking in a 1 M $LiPF_6$ Ethylene Carbonate/Dimethyl Carbonate 1:1 by volume mixture for 10 min:

$$\text{Electrolyte uptake} = \left(\frac{W_b - W_a}{W_a}\right) \times 100 \quad [1]$$

where W_a and W_b are the weights of separator before and after soaking in the electrolyte. A minimum of 3 replicas per membrane were measured.

Ionic conductivity.—We assembled CR2032 coin cells containing the separators in an Argon-filled glove-box. The membranes were punched into 15.9-diameter disks and the thickness was measured. The separator was placed between two stainless steel spacers in the cell can, 50 μl of 1 M $LiPF_6$ in EC/DMC (1:1 by volume) added, and the cell was crimped closed. We measured ionic resistance by electrochemical impedance spectroscopy (EIS) with a Bio-Logic VMP3 Potentiostat. The frequency sweeps ranged from 500 kHz to 1 Hz with an amplitude of 10 mV. The conductivity σ is calculated with Eq. 2:

$$\sigma = \frac{t}{R_{ion} \cdot A} \quad [2]$$

where t is the membrane thickness, R_{ion} is the measured ionic resistance (high-frequency intercept of Nyquist plot), and A is the membrane area. The conductivity was measured for 3 replicas per membrane in a temperature-controlled chamber.

Cell-cycling performance.—For rate capability and cycling measurements, we used the separators in a cell comprising a $LiCoO_2$ (Electrodes and More, Richardson, TX) cathode and Li metal anode, with 50 μl of 1 M $LiPF_6$-EC/DMC (1:1 v/v). Using the VMP3 potentiostat, we pre-cycled (conditioned) the cells between 3 V and 4.2 V at C/20 for 5 cycles and thereafter cycled the cells at C/10, C/5, C/2, and 1 C rates at room temperature. The cycling stability was obtained by cycling cells for 50 cycles at a C/5 rate. A minimum of 3 replicas per separator were assembled into coin cells and cycled to assess reproducibility.

Results and Discussion

Membrane fabrication.—At a concentration of 5 wt.% PVDF in the injection solution, the resulting particles have a characteristic highly branched, fibrous SDC structure (Figs. 1a–1c). An increase in the concentration to 12.5 wt.% PVDF in the injection solution results in the formation of thin, but highly porous nano-sheet (NS) particulates (Figs. 1g–1i). Particle morphology affects membrane formation during the filtration step. As the concentration of PVDF increased from 5% to 10 wt.%, the SEM images reveal that the membranes transition from an entirely fibrous network to a mixed-morphology to a nano-sheet morphology, with pore sizes ranging from 10 to 500 nm (Figs. 1c, 1f, 1i). At a PVDF concentration of

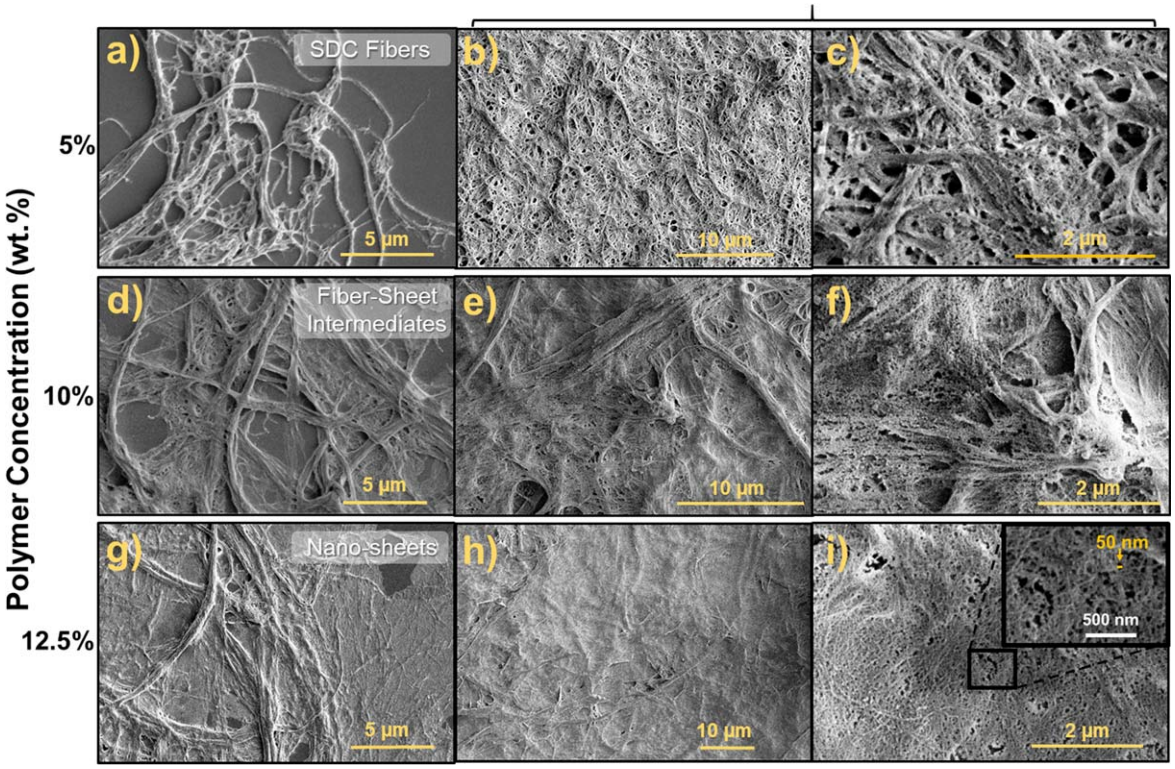

Figure 1. SEM images of SDC particles and the surface features of membranes fabricated therefrom. The images show a variation in particle morphologies and membrane features at different magnifications: fibrous (a)–(c); fibrous-nano-sheet (NS) (d)–(f); and NS membranes (g)–(i).

12.5 wt.%, the resulting particles are almost entirely sheet-like with few fibers present. Cross-sectional scanning electron micrographs revel that the membranes are of uniform thickness with a continuous pore network through the material (Fig. S1, supplemental material (available online at stacks.iop.org/JES/168/020517/mmedia)). SDC fibrous particles show a homogeneous, but wide distribution of pores (Fig. 1c), where pore size and distribution on the membrane surface and its cross-section are similar, as seen from Figs. 1 and S1. On the contrary, NS particles tend to assemble in a specific directional way, in which the nano-sheets are parallel to the membrane surface (Fig. 2). This organization creates a spatially homogeneous, wide pore-size distribution in the *x-y* direction (parallel to the membrane surface) but not in the *z* direction, leading to a surface more porous than the compact cross-section. The SEM images reveal that combination of fibers and nano-sheets in the mixed-morphology particulates create a disrupted pore network in all directions in the membrane with a narrow size distribution (Fig. 1f).

The transition of the particulate morphology from fibrous to sheet-like is supposed a result of the increase in polymer solution viscosity with increasing weight percent PDVF in the solution injected into the shear zone. The higher weight percent solutions require more energy for droplet deformation by the nonsolvent while maintaining a similar rate of polymer precipitation, resulting in the exfoliation of thin sheets at the solvent-nonsolvent interface at high PVDF concentration. Regardless of the particulates morphology, the PVDF suspensions can be filtered to form porous membranes with different and controllable thickness (15 μm minimum).

Thermal stability.—Thermal decomposition of the PVDF SDC membranes starts at ~450 °C (vs 350 °C for Celgard®) indicating high thermal stability (Fig. S2). PVDF SDC membranes showed 5.1% shrinkage after exposure to air at 90 °C for 1 h (5% shrinkage in machine direction for Celgard® 2500). The shrinkage at 130 °C and 150 °C was 8.5% and 16.2%, respectively. The results shown in Fig. S3 indicate that the membranes are stable at high temperatures (no wrinkles or folding) and the shrinkage is within battery operation guidelines (5% at 90 °C for 1 h).[40] Similar membranes composed of layered nanofibers of materials of differing melting temperatures have been utilized as active shutdown materials with the low-melting layer serving as a sacrificial, pore-filling material.[41–45] While SDCs membranes may be suitable for this purpose, we did not investigate layered separators in this study.

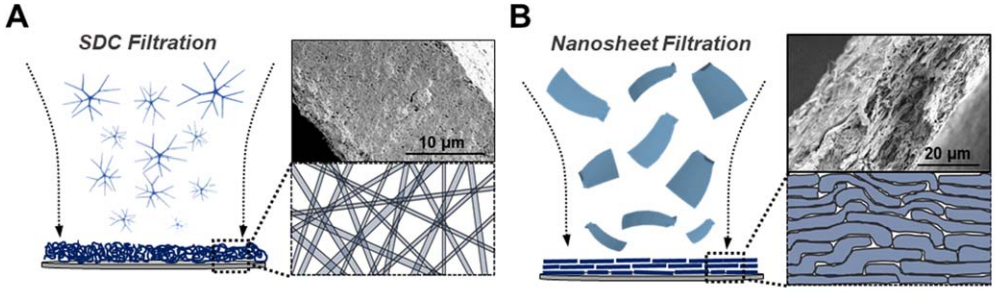

Figure 2. SEM of membrane cross-sections and schematic of the formation of (a) fibrous SDC membranes at 5 wt.% PVDF in DMSO, and (b) formation of NS membranes at 12.5 wt.% PVDF in DMSO.

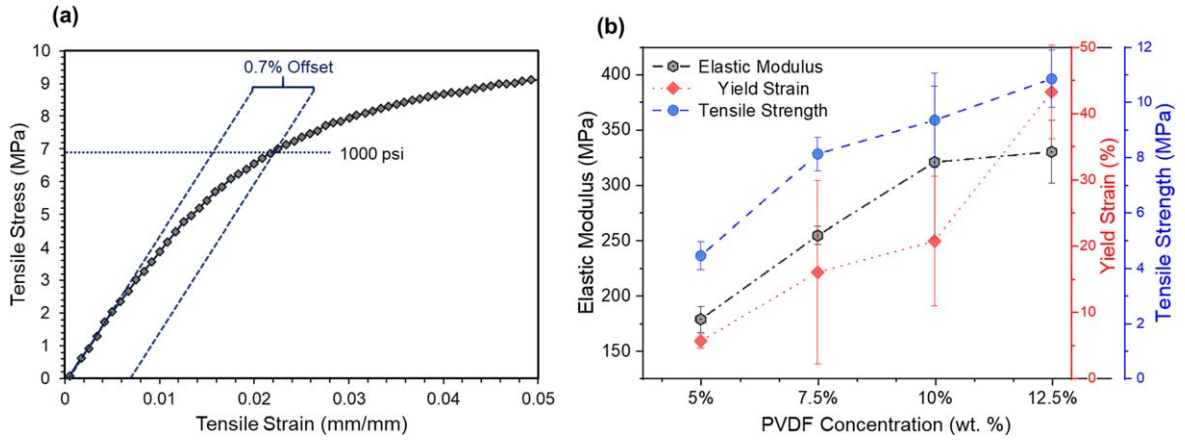

Figure 3. Mechanical properties of PVDF SDC membranes. (a) Stress-strain curve of a 48 μm thick PVDF SDC membrane. (b) Elastic modulus, elongation at break, and tensile strength of PVDF SDC membranes dependency on concentration of the injection solution for particle formation.

Table I. Number-average pore size (P_n), weight-average pore size (P_w), and heterogeneity index (HG = P_w/P_n) of PVDF SDC membranes.

Morphology	P_n (nm)	P_w (nm)	HG
SDC Fibrous	233	331	1.42
SDC Fibrous-NS	451	555	1.12
NS	286	426	1.49

Mechanical properties.—A typical stress-strain curve of a PVDF SDC membrane of fibrous-NS mixed-morphology particulates is shown in Fig. 3. These membranes have mechanical properties similar to those displayed by electrospun mats with elastic response and brittle fracture.[10] The elastic modulus of the material was 347 MPa, with >30% strain before fracture and just 0.7% offset at 1000 psi (yield stress is 5 MPa), which indicates these membranes seem suitable for roll-to-roll manufacturing. We established that as the concentration of PVDF in the injection solution increases, the elastic modulus, tensile strength, and elongation at break of the resulting membranes increase (Fig. 3b), indicating that the membranes with more sheet-like particle morphology are more mechanically robust than those with fibrous morphology.

The porosity of the SDC membranes is 70%–80% (Table II), which is higher than commercially available microporous separators (Celgard® 2500 porosity is 55%), and it is sufficient for obtaining a high electrolyte uptake and ionic conductivity while retaining mechanical integrity of the separator. Table I shows results for average pore size and heterogeneity of pore sizes for the SDC membranes. While it is often stated in the literature that a small pore size is preferable for favorable electrochemical performance, we noticed that the heterogeneity of pore sizes (hence the pore-size distribution) also plays an important role. In particular, separators made from the SDC fibrous-particulate morphology show the lowest pore size, but their pore-size distribution is wide (heterogeneity index, HG = 1.42); their conductivity is the highest among the three morphologies, and cells using these membranes retain capacity best during cycling, as discussed below. Separators made from the NS morphology particulates show a higher average pore size but a comparable distribution with a HG index equal to 1.49. Indeed, their performance in cells is slightly lower than cells using separators from the fibrous morphology particulates. The mixed-morphology membranes show a high average pore size and a narrow distribution, which seems to be detrimental to cell performance.

Electrochemical performance.—We observed that the fibers swell after imbibing the mat with liquid electrolyte, which is

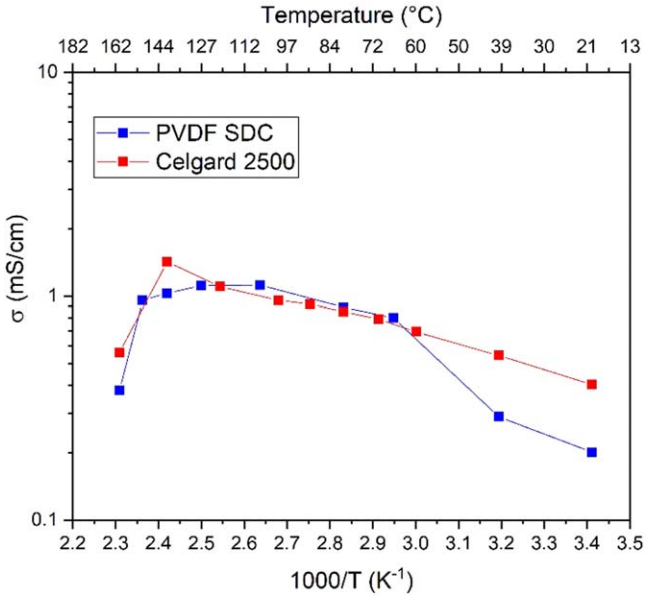

Figure 4. Conductivity of PVDF SDC fibrous-NS membranes and Celgard® 2500.

congruent with PVDF-electrolyte interactions reported elsewhere.[32] The electrolyte uptake of membranes prepared from particulates using the 5% PVDF injection solution was as much as 325%. The lower the fibrous morphology composition of the membranes, the lower was the electrolyte uptake, when assessed at approximately a similar porosity. The reason may be attributed to the higher surface area of membranes comprising fibrous morphology particulates, which absorb electrolyte in the outer surfaces of the fibers, compared to membranes comprising sheet-like morphologies (Table II).[32]

As with electrolyte uptake, the hierarchically fibrous morphology enhances the membrane conductivity (Table II). This is due to a higher surface area of the fibrous morphology membranes (and, speculatively, a greater fraction of PVDF amorphous phase[32]) compared to membranes comprising NS morphology particulates, both trends leading to a higher electrolyte uptake (Table II). The conductivity of PVDF SDC membranes is comparable to Celgard® membranes. At low temperatures, Celgard® has a slightly higher conductivity (except membranes with 5% initial PVDF concentration), but PVDF SDC membranes and Celgard® have comparable conductivities above 60 °C, with PVDF showing stability up to 150 °C, with a conductivity of 1 mS cm^{-1} (Fig. 4). We recognize at high temperatures (>90 °C), there is likely a two-phase mixture within the coin cell and possibly

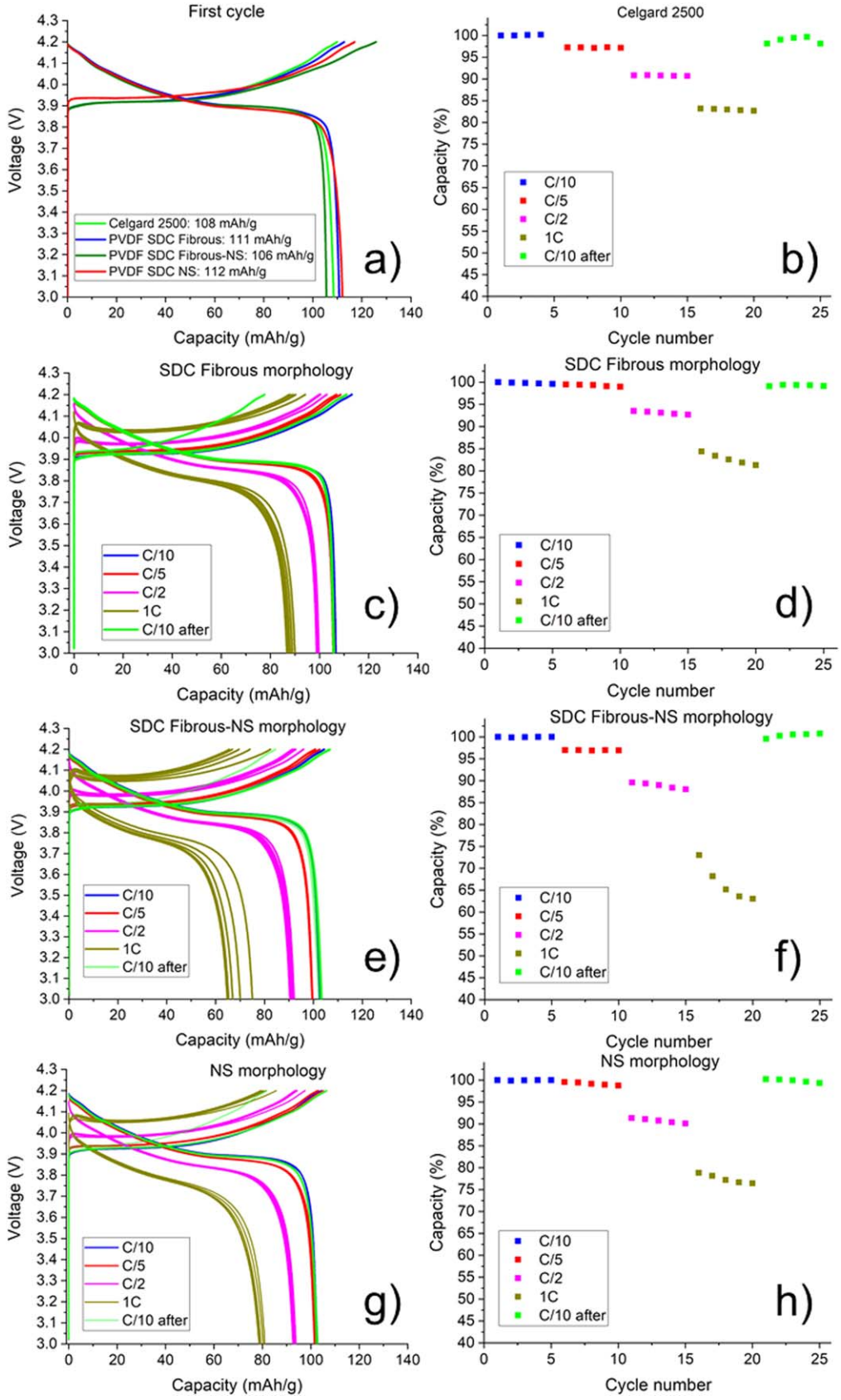

Figure 5. First-cycle capacity of Celgard® and PVDF SDCs membranes (a), charge-discharge curves and rate capability of cells containing Celgard® (b), PVDF SDC fibrous (c), (d), fibrous-NS (e), (f), and NS membrane separators (g), (h).

Table II. Thickness and conductivity of PVDF SDC membranes from particles prepared at differing PVDF concentrations in the injection solution.

Initial PVDF Concentration (wt.%)	Porosity (%)	Electrolyte Uptake (%)	Conductivity (mS cm^{-1})
5% (Fibrous)	78	325	1.21
7.5% (Fibrous)	77	250	0.78
10% (Fibrous-NS)	67	234	0.51
12.5% (NS)	76	238	0.56
Celgard®	55	70	0.94

thermally induced decomposition of the salt, but none of the cells lost their seal. We are also aware that typical batteries are not run at such high temperatures, but nonetheless these data help develop a better understanding of the SDC membranes.

The electrochemical stability of the SDC membranes was assessed by measuring the potential at which a current of 10 μA cm^{-2} was observed in a cell containing stainless steel electrodes (Fig. S4).[46] Although Celgard® has a higher oxidation limit (5 V), the limit for the PVDF SDC membranes (4.5 V) is sufficient to be compatible with most of the common materials used for lithium battery cathodes.[47–49]

Charge-discharge curves were obtained using the SDC separators in Li/$LiCoO_2$ coin cells. The first-cycle capacity was obtained at a C/20 discharge rate (Fig. 5a). With all separator morphologies, cells using PVDF SDC membranes showed a capacity similar or superior to Celgard® separators in the first cycle, with NS membranes showing a capacity of 112 mAh g^{-1}. Voltage hysteresis was calculated at 50% state-of-charge and was 2 mV for cells containing all separators (including Celgard) except for NS morphology, whose voltage hysteresis was 5 mV, indicating a slower Li transfer kinetics for NS morphology membranes. Charge-discharge curves show that the cells with fibrous PVDF SDC separators have the highest capacity for each rate of discharge (Fig. 5); however, these values are not significantly higher than capacity of cells containing separators with fibrous-NS or NS morphologies. The difference in capacity fade between cells containing separators with different morphologies increases at rates higher than C/2. For example, differently from cells with SDC fibrous morphology, cells containing SDC fibrous-NS separators show a significant capacity loss when switching from C/2 to 1 C rate, and the loss increases with each subsequent cycle at 1 C (Fig. 5).

A range of pore sizes is always present in nonwoven separators. The SDC membranes with largest pores and narrowest distribution among the 3 morphologies (i.e. fibrous-NS) are less suitable as battery separators (Table I). However, based upon the observations made with the SDC membranes with various morphologies, membranes with only small pores tend to have high resistance to the flow of liquids or ions; in this case small pores are mainly created by nanofibers, which weaken the web. The cumulative effects of large pores for strength and openness from microfibers scaffolding, small average pore size from a nanofiber net, and high number of pores for a high-porosity membrane combine to provide a superior structure for a Li-ion battery separator.

PVDF SDC separators and Celgard® have a similar rate capability (max charge/discharge rate) up to 1 C rate, and the capacity loss is <5% after cycling through C/10 to 1 C. A major benefit of PVDF SDC membranes is the simple chemical composition and production process. By tailoring the particle morphology of a single polymer, we are able to create a battery separator whose properties are similar or superior to commercial separators, which usually require additives or surfactants to increase their affinity with liquid electrolytes.[8]

To determine if these separators were capable of repeated cyclic use, 50 charge/discharge cycles were performed with cells containing PVDF SDC fibrous-NS separators (Fig. 6). Following 50 cycles of charge/discharge at a C/5 rate, the capacity of the cell decreased by ~10% (~1% capacity fade for Celgard®), while the coulombic efficiency is higher than 95%, which is comparable to Celgard® (99% efficiency). This capacity loss indicates that PVDF SDC membranes may have long-term chemical and electrochemical

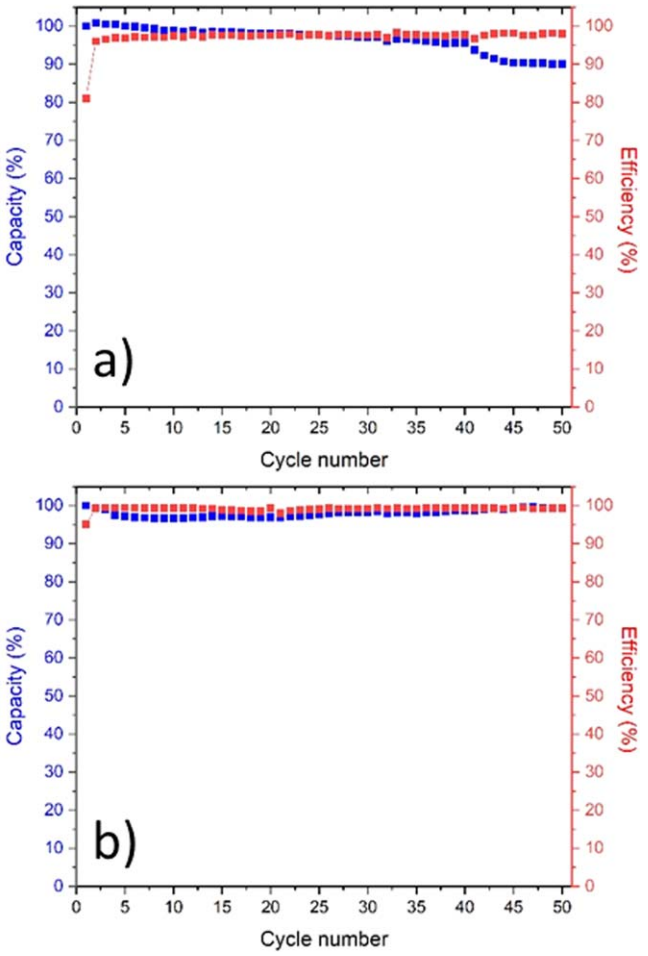

Figure 6. 50 Charge-discharge cycles of PVDF SDC fibrous-NS membrane separator (a) and Celgard (b) at C/5 rate in a Li/$LiCoO_2$ cell with 1 M $LiPF_6$ in EC/DMC 1:1%wt.

stability issues. However, top-view (Fig. S5) and cross-section (Fig. S6) SEM images of SDC membranes after cycling show no significant changes, revealing similar branched network and porosity as before cycling. Fig. S7 shows EIS spectra before and after cycling of cells containing all membranes, including Celgard®. Cells with fibrous and mixed morphology separators show little or no change in the ionic resistance after cycling, while cells with NS morphology show an increased resistance (from 6 to 10 Ω), which does not seem to affect the rate capability measurements.

The three different morphologies of SDC membranes found in this work have advantages in different properties. The SDC fibrous morphology (obtained with a low PVDF concentration in injection solutions) has small mean-pore size, high surface and electrolyte uptake, and high rate capability. The closer the particles are to fibrous morphology, the lower is the mean pore size, but the pore-size distribution is wider. The heterogeneity of pore sizes creates strong and better-performing membranes, with high electrolyte

uptake and conductivity. Even though the SDC fibrous mats showed the best electrochemical performance, all morphologies showed performance comparable to Celgard®.

Conclusions

Shear-driven polymer precipitation offers a new method of producing porous membranes. This method could be conveniently and efficiently adapted for producing battery separators not only because of the scalability of the process, but also the versatility by which nanofibrous and sheet-like particles can be produced from a variety of polymers. The ability to produce these extremely high aspect ratio particles from different polymers allows the facile formation of membranes with a network of fibers or sheets tortuous enough for electrochemical stability in LIBs, but also porous enough for high conductivity. The cells containing fibrous morphology membranes (low initial PVDF concentration in the injection solution) showed a high conductivity, capacity, and charge/discharge rate capability, while the sheet-like membranes showed better mechanical properties. The morphology of the membranes determines the performance and can be adjusted to the specific application, e.g., by layering or mixing particles of the two distinct morphology. The versatility of the process allows for multiple polymer precipitation and for incorporation of additives, such as ceramic particles, for composite separators. However, we have shown that even with a single polymer the structure of the pore network is a key factor in making these membranes competitive LIB separators.

Acknowledgments

The authors gratefully acknowledge support from US National Science Foundation, no. CMMI-1825476 and from North Carolina State University.

ORCID

Salvatore Luiso https://orcid.org/0000-0002-9793-0444
Austin H. Williams https://orcid.org/0000-0003-4080-5164
Michael J. Petrecca https://orcid.org/0000-0002-7111-3526
Orlin D. Velev https://orcid.org/0000-0003-0473-8056
Peter S. Fedkiw https://orcid.org/0000-0003-4171-036X

References

1. J. Tarascon and M. Armand, "Issues and challenges facing rechargeable lithium batteries." *Nature*, **414**, 359 (2001).
2. M. Yang and J. Hou, "Membranes in lithium ion batteries." *Membranes*, **2**, 367 (2012).
3. C. Pillot, "The rechargeable battery market and main trends 2017- 2025." *Avicenne Energy.* (2018).
4. M. F. Lagadec, R. Zahn, and V. Wood, "Characterization and performance evaluation of lithium-ion battery separators." *Nat. Energy*, **4**, 16 (2019).
5. V. Deimede and C. Elmasides, "Separators for lithium-ion batteries: a review on the production processes and recent developments." *Energy Technol*, **3**, 453 (2015).
6. C. M. Costa, Y. H. Lee, J. H. Kim, S. Y. Lee, and S. Lanceros-Méndez, "Recent advances on separator membranes for lithium-ion battery applications: from porous membranes to solid electrolytes." *Energy Storage Mater.*, **22**, 346 (2019).
7. S. Luiso and P. S. Fedkiw, "Lithium-ion battery separators: recent developments and state of art." *Curr Opin Electrochem*, **20**, 99 (2020).
8. K. M. Abraham, M. Alamgir, and D. K. Hoffman, "Polymer electrolytes reinforced by celgard® membranes." *J. Electrochem. Soc.*, **142**, 683 (1995).
9. A. A. Heidari and H. Mahdavi, "Recent development of polyolefin-based microporous separators for li−ion batteries: a review." *Chem. Rec.*, **20**, 570 (2020).
10. Y. Li, Q. Li, and Z. Tan, "A review of electrospun nanofiber-based separators for rechargeable lithium-ion batteries." *J. Power Sources*, **443**, 227262 (2019).
11. K. Song et al., "Electrospun PU/PVP/GO Separator for Li-ion Batteries." *Fibers Polym.*, **20**, 961 (2019).
12. Z. Liang, Y. Zhao, and Y. Li, "Electrospun core–shell nanofiber as separator for lithium-ion batteries with high performance and improved safety." *Energies*, **12**, 3391 (2019).
13. L. Wang, Z. Wang, Y. Sun, X. Liang, and H. Xiang, "Sb_2O_3 modified PVDF-CTFE electrospun fibrous membrane as a safe lithium-ion battery separator." *J Memb Sci.*, **572**, 512 (2019).
14. H. Wen, J. Zhang, J. Chai, J. Ma, L. Yue, T. Dong, X. Zang, Z. Liu, B. Zhang, and G. Cui, "Sustainable and superior heat-resistant alginate nonwoven separator of $LiNi_{0.5}Mn_{1.5}O_4$/Li batteries operated at 55 °C." *ACS Appl. Mater. Interfaces,*, **9**, 3694 (2017).
15. E. Shekarian, M. R. J. Nasr, T. Mohammadi, O. Bakhtiari, and M. Javanbakht, "Enhanced wettability and electrolyte uptake of coated commercial polypropylene separators with inorganic nanopowders for application in lithium-ion battery." *J Nanostruct.*, **9**, 736 (2019).
16. H. Lee et al., "Preparation and characterization of electrospun nanofiber-coated membrane separators for lithium-ion batteries." *J. Solid State Electrochem.*, **18**, 2451 (2014).
17. C. Yang, Z. Jia, Z. Guan, and L. Wang, "Polyvinylidene fluoride membrane by novel electrospinning system for separator of Li-ion batteries." *J. Power Sources*, **189**, 716 (2009).
18. J. L. Pan, Z. Zhang, H. Zhang, P. P. Zhu, J. C. Wei, J. X. Cai, J. Yu, N. Koratkar, and Z. Y. Yang, "Ultrathin and strong electrospun porous fiber separator." *ACS Appl. Energy Mater.*, **1**, 4794 (2018).
19. Y. Zhu, M. Yin, H. Liu, B. Na, R. Lv, B. Wang, and Y. Huang, "Modification and characterization of electrospun poly (vinylidene fluoride)/poly (acrylonitrile) blend separator membranes." *Compos Part B Eng*, **112**, 31 (2017).
20. J. C. Barbosa, J. P. Dias, S. Lanceros-Méndez, and C. M. Costa, "Recent advances in poly(Vinylidene fluoride) and its copolymers for lithium-ion battery separators." *Membranes*, **8**, 45 (2018).
21. S.-S. Choi, Y. S. Lee, C. W. Joo, S. G. Lee, J. K. Park, and K.-S. Han, "Electrospun PVDF nanofiber web as polymer electrolyte or separator." *Electrochim. Acta*, **50**, 339 (2004).
22. M. Waqas, S. Ali, C. Feng, D. Chen, J. Han, and W. He, "Recent development in separators for high-temperature lithium-ion batteries." *Small*, **15**, 1901689 (2019).
23. K. Bicy, S. Suriyakumar, P. Anu Paul, A. S. Anu, N. Kalarikkal, A. M. Stephen, V. G. Geethamma, D. Rouxel, and S. Thomas, "Highly lithium ion conductive, Al_2O_3 decorated electrospun P(VDF-TrFE) membranes for lithium ion battery separators." *New J. Chem.*, **42**, 19505 (2018).
24. S. Yang, W. Ma, A. Wang, J. Gu, and Y. Yin, "A core–shell structured polyacrylonitrile@poly(vinylidene fluoride-hexafluoro propylene) microfiber complex membrane as a separator by co-axial electrospinning." *RSC Adv.*, **8**, 23390 (2018).
25. B. Boateng, G. Zhu, W. Lv, D. Chen, C. Feng, M. Waqas, S. Ali, K. Wen, and W. He, "An efficient, scalable route to robust PVDF-co-HFP/SiO_2 separator for long-cycle lithium ion batteries." *Phys. Status Solidi RRL*, **12**, 1800319 (2018).
26. Y. Xiang, W. Zhu, W. Qiu, W. Guo, J. Lei, D. Liu, D. Qu, Z. Xie, H. Tang, and J. Li, "SnO_2 Functionalized polyethylene separator with enhanced thermal stability for high performance lithium ion battery." *ChemistrySelect*, **3**, 911 (2018).
27. H. Qu et al., "Inorganic separators enable significantly suppressed polysulfide shuttling in high-performance lithium–sulfur batteries." *J. Mater. Chem. A*, **6**, 23720 (2018).
28. H. Gao, Y. Chen, H. Sun, A. Zhao, L. Wang, and N. Liu, "Silicone modified polypropylene separator for high temperature lithium ion battery applications." *Mater. Res. Express*, **5**, 065512 (2018).
29. C. Y. Chao, Y. F. Feng, K. Hua, H. Li, L. J. Wu, Y. S. Zhou, and Z. W. Dong, "Enhanced wettability and thermal stability of polypropylene separators by organic–inorganic coating layer for lithium-ion batteries." *J. Appl. Polym. Sci.*, **135**, 46478 (2018).
30. S. P. Herle and J. G. Gordon, "Ceramic coating on battery separators." (2019), US Patent 10193116B2, Washington, DC: U.S. Patent and Trademark Office.
31. Y. Han, L. Ye, B. Boateng, Q. Sun, C. Zhen, N. Chen, X. Shi, J. H. Dickerson, X. Li, and W. He, "Direct electrophoretic deposition of an ultra-strong separator on an anode in a surfactant-free colloidal system for lithium ion batteries." *J. Mater. Chem. A*, **7**, 1410 (2019).
32. S. Luiso, J. J. Henry, B. Pourdeyhimi, and P. S. Fedkiw, "Fabrication and characterization of meltblown poly(vinylidene difluoride) membranes." *ACS Appl Polym Mater*, **2**, 2849 (2020).
33. R. Luo, C. Wang, Z. Zhang, W. Lv, Z. Wei, Y. Zhang, X. Luo, and W. He, "Three-dimensional nanoporous polyethylene-reinforced PVDF-HFP separator enabled by dual-solvent hierarchical gas liberation for ultrahigh-rate lithium ion batteries." *ACS Appl. Energy Mater.*, **1**, 921 (2018).
34. J. Liu, X. Shi, B. Boateng, Y. Han, D. Chen, and W. He, "A highly stable separator from an instantly reformed gel with direct post-solidation for long-cycle high-rate lithium-ion batteries." *ChemSusChem*, **12**, 908 (2019).
35. L. Ye, X. Shi, Z. Zhang, J. Liu, X. Jian, M. Waqas, and W. He, "An efficient route to polymeric electrolyte membranes with interparticle chain microstructure toward high-temperature lithium-ion batteries." *Adv. Mater. Interfaces*, **4**, 1601236 (2017).
36. B. Liu, Y. Huang, L. Zhao, Y. Huang, A. Song, Y. Lin, M. Wang, X. Li, and H. Cao, "A novel non-woven fabric supported gel polymer electrolyte based on poly(methylmethacrylate-polyhedral oligomeric silsesquioxane) by phase inversion method for lithium ion batteries." *J Memb Sci*, **564**, 62 (2018).
37. O. D. Velev, S. Smoukov, P. Geisen, M. C. Wright, and S. Gangwal, "Method for fabricating nanofibers." (2015), US Patent US9217211B2 Washington, DC: U.S. Patent and Trademark Office.
38. O. D. Velev, S. Smoukov, and M. Marquez, "Nanospinning of polymer fibers from sheared solutions." (2013), US Patent US8551378, Washington, DC: U.S. Patent and Trademark Office.
39. O. D. Velev and S. Roh, "Fractal-like polymeric particles and their use in diverse applications." (2017), WIPO patent WO2017196864A1.
40. S. Roh, A. H. Williams, R. S. Bang, S. D. Stoyanov, and O. D. Velev, "Soft dendritic microparticles with unusual adhesion and structuring properties." *Nat. Mater.*, **18**, 1315 (2019).
41. H. Lee, M. Yanilmaz, O. Toprakci, K. Fu, and X. Zhang, "A review of recent developments in membrane separators for rechargeable lithium-ion batteries." *Energy Environ. Sci.*, **7**, 3857 (2014).

42. C. Shi, P. Zhang, S. Huang, X. He, P. Yang, D. Wu, D. Sun, and J. Zhao, "Functional separator consisted of polyimide nonwoven fabrics and polyethylene coating layer for lithium-ion batteries." *J. Power Sources*, **298**, 158 (2015).
43. Z. Li, Y. Xiong, S. Sun, L. Zhang, S. Li, X. Liu, Z. Xu, and S. Xu, "Tri-layer nonwoven membrane with shutdown property and high robustness as a high-safety lithium ion battery separator." *J Memb Sci.*, **565**, 50 (2018).
44. Y. Li and H. Pu, "Facile fabrication of multilayer separators for lithium-ion battery via multilayer coextrusion and thermal induced phase separation." *J. Power Sources*, **384**, 408 (2018).
45. Y. Li, H. Pu, and Y. Wei, "Polypropylene/polyethylene multilayer separators with enhanced thermal stability for lithium-ion battery via multilayer coextrusion." *Electrochim Acta,*, **264**, 140 (2018).
46. H. S. Choe, B. G. Carroll, D. M. Pasquariello, and K. M. Abraham, "Characterization of some polyacrylonitrile-based electrolytes." *Chem. Mater.*, **9**, 369 (1997).
47. X. Li, G. Cheruvally, J. K. Kim, J. W. Choi, J. H. Ahn, K. W. Kim, and H. J. Ahn, "Polymer electrolytes based on an electrospun poly(vinylidene fluoride-co-hexafluoropropylene) membrane for lithium batteries." *J. Power Sources*, **167**, 491 (2007).
48. G. Cheruvally et al., "Electrospun polymer membrane activated with room temperature ionic liquid: novel polymer electrolytes for lithium batteries." *J. Power Sources*, **172**, 863 (2007).
49. L. Wang, J. Ma, C. Wang, X. Yu, R. Liu, F. Jiang, X. Sun, A. Du, X. Zhou, and G. Cui, "A novel bifunctional self-stabilized strategy enabling 4.6 V $LiCoO_2$ with excellent long-term cyclability and high-rate capability." *Adv. Sci.*, **6**, 1900355 (2019).